Macromolecules

pubs.acs.org/Macromolecules Article

Synergistic Radical Taming by Concurrent Degenerative Transfer and Atom Transfer Radical Polymerization in Emulsion

Francesco De Bon,* Teresa J. Lourenço Bernardino, Arménio Coimbra Serra, Marco Fantin, Krzysztof Matyjaszewski, and Jorge Fernando Jordao Coelho

Cite This: *Macromolecules* 2024, 57, 10297−10310 Read Online

ACCESS | Metrics & More | Article Recommendations | Supporting Information

ABSTRACT: Atom transfer radical polymerization (ATRP) and reversible addition−fragmentation chain transfer polymerization (RAFT) are two independent polymer synthesis methods. Here, we show that the synergy between the ATRP and RAFT degenerative transfer mechanisms under emulsion conditions is a promising and attractive option for scalable and efficient polymerization processes, offering significant advantages over stand-alone procedures. They work synergistically, reinforcing each other and relaxing the stringent conditions required for controlled radical polymerization in emulsion. This drastically reduces the metal loading and environmental impact. Stable, well-defined latexes of poly(*n*-butyl methacrylate) with predetermined molecular weights and $Đ < 1.5$ were obtained with only 50 μM Cu (18.3 ppm) on a 1 L scale and even below this concentration on a 20 mL scale. The latex color imparted by the RAFT chain transfer agent was catalytically decolorized by a one-pot, nondisruptive method using an ATRP Cu catalyst via the oxygen reduction reaction (ORR).

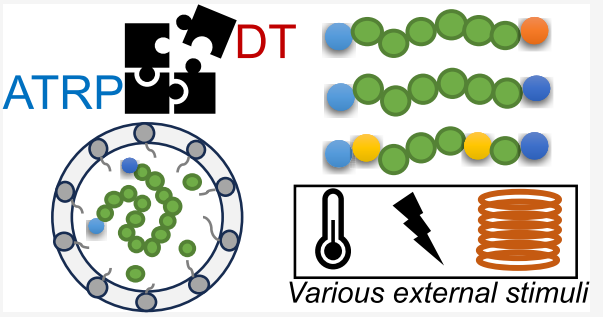

1. INTRODUCTION

The synthesis of polymers with tailored properties is a topic of great interest to both academia and industry. Various techniques from the reversible deactivation radical polymerization (RDRP) family[1] enable the preparation of polymers with controlled molecular weights, narrow molecular weight distributions, precise compositions, functionalities, and architectures, all of which have a significant impact on the resulting polymer properties.[2−4] RDRPs are used to produce various materials such as coatings, adhesives, vibration damping materials, inks, detergents, paints, surfactants, and many others.[5−7] Among RDRPs, atom transfer radical polymerization (ATRP)[8−13] and reversible addition−fragmentation chain transfer (RAFT)[4,14−18] are the most widely used techniques, both of which are suitable for the preparation of well-defined materials. However, the choice between the two methods is often arbitrary, depending on user experience, or is simply based on the researcher's previous work.[19] Both possess unique strengths and weaknesses and are recognized as distinct methods.[1,20,21] The simultaneous use of more than one mechanism to tame radicals within the same polymerization process has received comparatively little attention to date. Although not initially obvious, ATRP and RAFT share fundamental mechanistic aspects. Scheme 1 summarizes the mechanisms of RAFT (under degenerative transfer, DT), ATRP with alkyl halides, ATRP with pseudohalides, and concurrent ATRP/DT (the focus of this work) for methacrylates.

All of the polymerization methods in Scheme 1 rely on radical-transferable groups. In ATRP, the halogen atom is the transferable group, and the reaction is catalyzed by Cu complexes. Alkyl bromides and chlorides serve as efficient ATRP initiators, whereas alkyl fluorides pose challenges because of their high R−F bond energy, resulting in slow activation and exchange between active and dormant species.[22] On the other hand, alkyl iodides can be used in both ATRP and DT processes.[23,24] In RAFT, certain chain transfer agents (CTAs) exhibit pseudohalogen behavior, such as dithioesters, and can be activated and transferred by Cu catalysts.[25−28] Depending on the monomer and alkyl pseudohalide combination, they may only act as ATRP initiators,[26] CTAs, or both. For example, while an alkyl dithiocarbamate (R-DC) can be activated by an ATRP catalyst and behave as a pseudohalide, its low activity and slow chain transfer make it unsuitable as a CTA for the RAFT polymerization of methacrylates.[28] A polymerization process in which both mechanisms operate concurrently,[29,30] referred to as ATRP/DT polymerization, relies on the rapid activation of an alkyl halide (R-Br) by a Cu catalyst (ATRP), supplemented by

Received: July 30, 2024
Revised: September 18, 2024
Accepted: September 27, 2024
Published: October 15, 2024

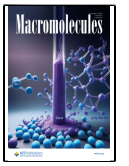

Scheme 1. Mechanisms of RAFT, Classic ATRP with Alkyl Halides, ATRP with Pseudohalides, and Differentiation between the Mechanisms[a]

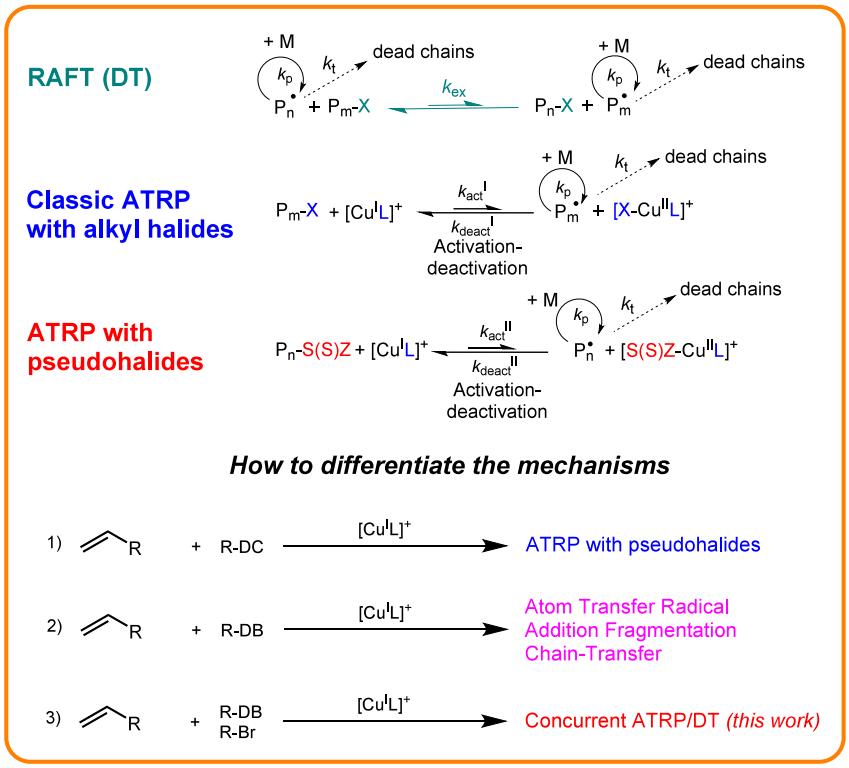

[a]M is the monomer; k_{act}, k_{deact}, and k_p are the activation, deactivation, and propagation rate constants, respectively; and k_t is the rate constant of radical termination. k_{act}^{I} and k_{deact}^{I} are the activation and deactivation rate constants, respectively, for the reaction between the copper catalyst and the C−Br bond, while k_{act}^{II} and k_{deact}^{II} are the activation and deactivation rate constants for the C−DB bond; k_{ex} is the exchange constant of the degenerative chain transfer. R-DC refers to an alkyl dithiocarbamate that behaves as a pseudohalide, and R-DB denotes an alkyl dithiobenzoate.

an additional control of radical growth by DT through a suitable CTA (such as a dithioester, R-DB). The mechanism of the combined DT/ATRP is presented in Scheme 2.

Aqueous emulsion polymerization is an ideal platform for studying and developing ATRP/DT polymerization. Emulsions are very important for industrial polymer synthesis because they allow the large-scale synthesis of hydrophobic polymers,[31−38] where the use of organic solvents is economically and environmentally unfeasible. Both ATRP and RAFT have been developed independently for emulsion polymerization, with each having its own limitations.[39] For example, early attempts with dithiobenzoates in *ab initio* batch emulsions resulted in broad or multimodal molar mass distributions, considerable retardation, inhibition, and poor latex stability.[40] The use of surfactant-free polymerizations with amphiphilic macroRAFT agents, predominantly trithiocarbonates, has significantly improved this aspect.[4,15−18,41−44] ATRP in emulsions has stringent requirements, with only a limited selection of ligands, initiators, and surfactants that are currently deemed suitable. How can ATRP/DT polymerization be integrated into an emulsion? We were inspired by photoATRP in emulsion (sometimes called *ab initio* emulsion), where the highly hydrophobic dodecyl methacrylate is shuttled through the aqueous phase to micelles or particles by the less hydrophobic *n*-butyl methacrylate (BMA).[45,46] Similarly, a hydrophobic CTA can enter polymerized particles and react with propagating radicals.

Scheme 2. Proposed Mechanism for Concurrent ATRP/DT[a]

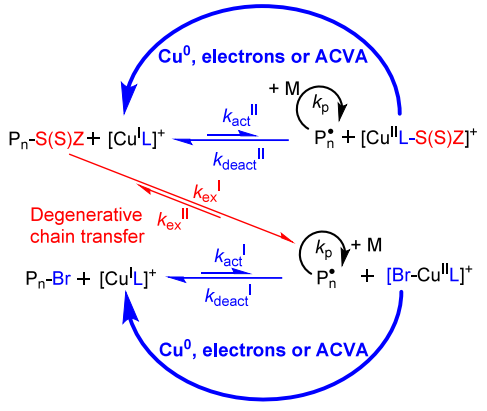

[a]Radical termination pathways have been omitted for clarity. k_{act}, k_{deact}, and k_p denote the activation, deactivation, and propagation rate constants, respectively. k_{act}^{II} and k_{deact}^{II} are the activation and deactivation rate constants for the C−S(S)Z (C−DB in this work) bond, while k_{act}^{I} and k_{deact}^{I} are the activation and deactivation rate constants for the C−Br bond, respectively. k_{ex}^{I} and k_{ex}^{II} are the exchange rate constants for the degenerative chain transfer.

In addition to the main polymerization equilibria, the Cu catalyst is also involved in the molecular oxygen reduction reaction (ORR) that converts O_2 to H_2O_2, which in turn is degraded by sodium pyruvate (SP) to CO_2, sodium acetate, and H_2O.[47] ORR in the presence of sodium pyruvate enables oxygen tolerance in ATRP.[48−50] This allowed us to develop and exploit

https://doi.org/10.1021/acs.macromol.4c01812
Macromolecules 2024, 57, 10297−10310

Scheme 3. Ligands, CTA, Alkyl Halides, And Conventional Radical Initiators That Were Used in This Work

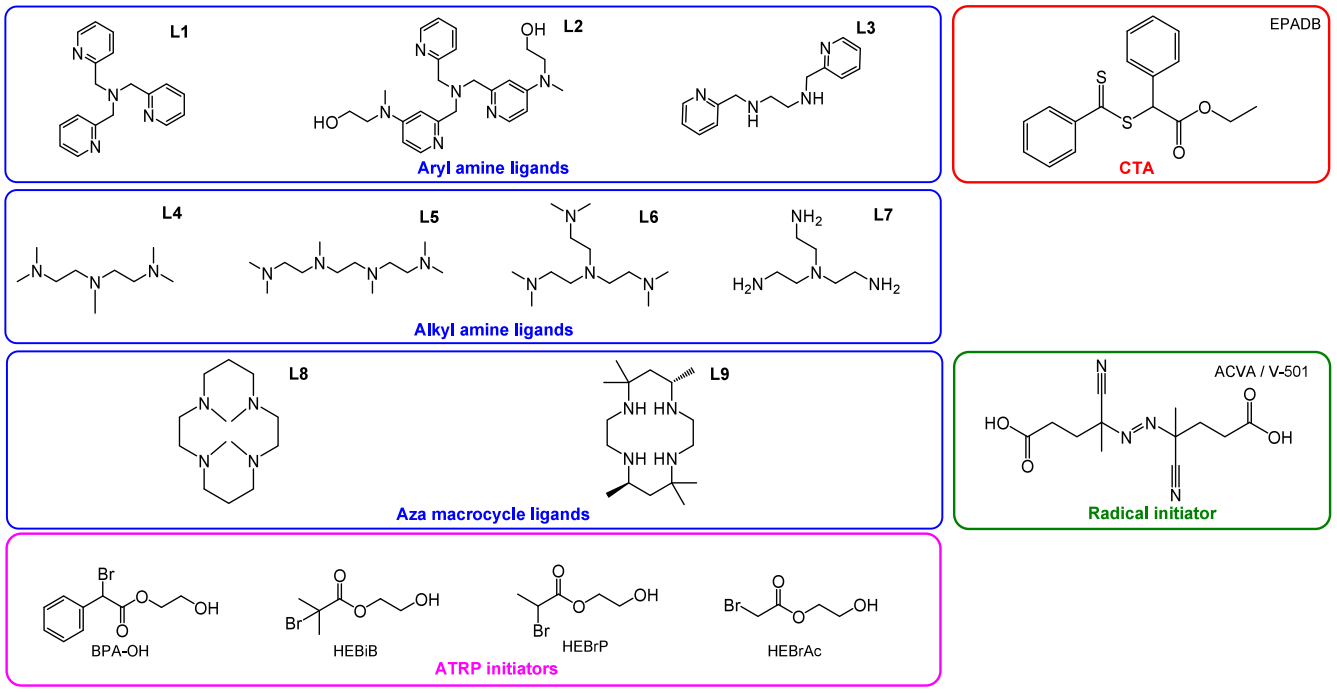

ATRP/DT polymerization in an emulsion without degassing and in the presence of a monomer inhibitor.

We will demonstrate the compatibility of ATRP/DT with various Cu complexes (*e.g.*, amine ligands, as shown in Scheme 3), explore the feasibility of reducing C_{Cu} to the micromolar range, and demonstrate the scale-up of ATRP/DT polymerization to 1 L using only 50 μM Cu catalyst.

2. RESULTS AND DISCUSSION

2.1. ATRP/DT Polymerization under Emulsion Conditions: Requirements. Polymethacrylates exhibit good mechanical properties, increased stiffness, durability, and resistance to deformation, making them attractive for applications that require high-performance materials. We chose BMA as the monomer to develop ATRP/DT in emulsions because of its near-room-temperature (~20 °C) glass transition temperature and relatively low water solubility. Considering ATRP and RAFT separately, in ATRP, the growth of PBMA is effectively controlled through the transfer of a halogen atom using a suitable catalyst, such as $[Cu^{II}TPMA]^{2+}$.[51] In RAFT dithiobenzoates, such as hydrophobic CTA ethyl 2-phenyl-2-((phenylcarbonothioyl)thio)acetate (EPADB), can effectively control the polymerization of methacrylates. EPADB has Z = Ph and R = $C_2H_5CO_2Ph$. The synthesis is described in detail in Supporting Information section S4.1, Figures S1−S6, and was inspired by earlier works by Hawker[52] and Lewis[53] through the alkylation of a dithiobenzoate salt with ethyl α-bromophenylacetate.[54] EPADB acts as a reactive secondary dithioester equipped with stabilizing phenyl and ester groups that ensure efficient reinitiation of methacrylates.[5455,56]

The hydrophobicity of EPADB makes it soluble in BMA droplets during polymerization, preventing its possible hydrolysis by contact with the water phase. However, during polymerization, EPADB must diffuse from the BMA into the aqueous phase. The EPADB must also be shielded from light exposure. Indeed, dithiobenzoates can trigger photoinduced electron transfer RAFT (PET-RAFT) when irradiated in the 380−600 nm range[57,58] through the spin-forbidden n → π^* electronic transition.[59] Fluorescent laboratory lighting can accelerate this unwanted polymerization process.[61] For this reason, we used BMA without removing the inhibitor (hydroquinone and HQ) and turned off the fume hood light. HQ traps unwanted radicals generated by exposure to ambient light.

Dithiobenzoates are more easily hydrolyzed under basic conditions,[60] whereas a slightly acidic aqueous phase (pH = 5.0) remains compatible with most amine ligands[62] and EPADB. The aqueous phase consisted of 10^{-2} M phosphate buffer at pH 5, sodium dodecyl sulfate (SDS) anionic surfactant, and a hydrophilic $[Cu^{II}L]^{2+}$ complex (where L is the amine ligand) serving as the ATRP catalyst, with NaBr and sodium pyruvate as cocatalysts. Radical initiation and nucleation occurred in the aqueous phase via the ATRP mechanism, facilitated by using a hydrophilic catalyst and initiator.[45,51,63−66] In ATRP, in emulsion, the catalyst is shuttled in and out from polymerizing particles by the dodecyl sulfate anion (SDS), and the conversion and $Đ$ depend on the SDS concentration.[48,64,65,74]

2.1.1. ATRP/DT Polymerization in Emulsions: Electrochemical Characterization. We conducted electrochemical analyses before initiating polymerization to assess the response of $[Cu^{II}TPMA]^{2+}$ and EPADB to the reaction environment (see Figure 1 and Figures S13−S20). Cyclic voltammetry (CV) revealed a slight negative shift in the redox wave for the $[Cu^{II}TPMA]^{2+}$ complex upon the addition of SP, indicating weak binding of SP, primarily to the Cu^{II} oxidation states. Despite the potential competition between SP and Br^- anions for the Cu^{II} coordination site, effective deactivation was maintained due to the low affinity constants for both ions.[47,50,67]

Upon the addition of 28 mM SDS (above the CMC of ~10 mM), the electrochemical response of $[Cu^{II}TPMA]^{2+}$ underwent further changes. $[Cu^{II}TPMA]^{2+}$ was further stabilized by the dodecyl sulfate anion via ion pairing,[68,69] which shifted the voltammetry to a more negative potential. The diminished cathodic and anodic currents were caused by the lower diffusion

https://doi.org/10.1021/acs.macromol.4c01812
Macromolecules 2024, 57, 10297−10310

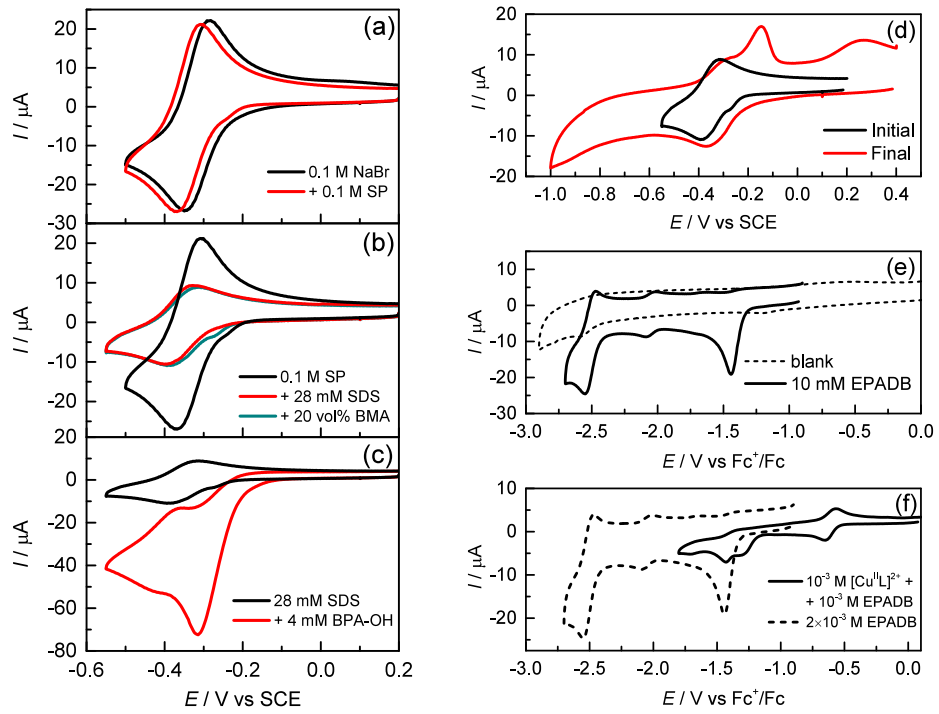

Figure 1. CV of 10^{-3} M $[Cu^{II}TPMA]^{2+}$ in H_2O + 0.1 M NaBr (a) before (black line) and after adding 0.1 M sodium pyruvate (red line); (b) after the addition of 28 mM sodium dodecyl sulfate (red line) after adding 20 vol % BMA containing 4 mM EPADB (green line), which saturated the aqueous phase; and (c) after adding 4×10^{-3} M 2-hydroxyethyl α-bromophenylacetate (red line). (d) CV of 10^{-3} M $[Cu^{II}TPMA]^{2+}$ before (black line) and at the end of the polymerization (red line). (e) CV of 10^{-3} M EPADB in DMF + 0.1 M Et_4NBF_4 (solid black line) against the blank (black dashed line). (f) CV 10^{-3} M $[Cu^{II}TPMA]^{2+}$ in the presence of 10^{-3} M EPADB (solid black line) in DMF + 0.1 M Et_4NBF_4; the CV of EPADB (black dashed line) is shown for comparison. All CVs were recorded on a GC disk electrode at a scan rate of 0.2 V/s at T = 25 °C under N_2 atmosphere.

coefficients when the catalyst was bound to micelles[68] (Figure 1b). This indicates that the deactivator was attracted to the micelles.

The addition of BMA (containing 4 mM EPADB) to the top of the aqueous phase saturated it with BMA (its aqueous solubility is 2.5 mM at T = 50 °C[31,70]). This resulted in a slight shift of the catalyst signal to more positive potentials (Figure 1b) owing to a small change in the polarity of the medium.

The introduction of the hydrophilic initiator 2-hydroxyethyl α-bromophenylacetate (BPA−OH, see section S3.1.2 of the Supporting Information) significantly altered the electrochemical response, with a large cathodic current observed as well as peak splitting (Figure 1c). The peak splitting into a catalytic peak followed by a reversible peak couple of the catalyst indicated the "total catalysis" regime,[71] indicating the extremely high activity of $[Cu^{I}TPMA]^{+}$ in this complex polymerization environment.

We conducted CV of EPADB in DMF + 0.1 M Et_4NBF_4 because of its limited aqueous solubility (Figure 1e); its electrochemical behavior was consistent with earlier reports on dithioester CTAs, showing an irreversible peak at about −1.5 V vs Fc^{+}/Fc.[72,73]

The CV of $[Cu^{II}TPMA]^{2+}$ in the presence of EPADB showed no increase in the cathodic current (Figure 1f), unlike that of BPA−OH, indicating that the Cu catalyst could not activate the DB pseudohalide chain end, at least in DMF. This suggests that in the presence of both Cu catalysts and EPADB, ATRP activation of RBr provided radicals for DT exchange. Based on these electrochemical findings, we investigated ATRP/DT polymerization.

2.3. ATRP/DT Polymerization under Emulsion Conditions: Effect of C_{Cu}.

Our polymerization setup, illustrated in Figure 2, involves comproportionation (supplemental activation and reducing agent, SARA) between Cu^{II} and Cu^{0} as a simple method to produce Cu^{I} and drive polymerization. A short 1.4 cm Cu^{0} wire (S_{Cu} = 0.44 cm^2, S_{Cu}/V = 0.022 cm^{-1}) was carefully dropped into the aqueous phase to initiate the reaction. Polymerization was initiated by the reaction of Cu^{I} with BPA−OH in the aqueous phase.

Our setup differed from traditional emulsion setups in that the aqueous phase and BMA (with EPADB) were initially separated (Figure 2a), allowing easy visualization of the EPADB mass transport. Emulsion processes using pre-emulsified monomers have not yet been attempted. During polymerization, the poorly water-soluble EPADB and BMA slowly diffused into the aqueous phase, forming a pale pink stable latex of PBMA (Figure 2).

During polymerization, the size exclusion chromatography (SEC) traces shifted smoothly toward higher molecular weights (Figure 2d), indicating a well-defined ATRP/DT process. The incorporation of the dithiobenzoate chain end into PBMA was detected by SEC using a UV detector set at 310 nm. Polymerization proceeds with reactivation of both the C−Br and C−DB chain ends. In the SEC measurements, the refractive index response was proportional to the PBMA mass (Figure 2d), whereas the UV response was proportional to the number of chains (Figure 2e), resulting in a more intense UV response for shorter chains.

Low catalyst loading is crucial for emulsions due to the toxicity and coloring effects of Cu catalysts.[74] We conducted polymerizations with decreasing Cu amounts (Table 1), from

https://doi.org/10.1021/acs.macromol.4c01812
Macromolecules 2024, 57, 10297−10310

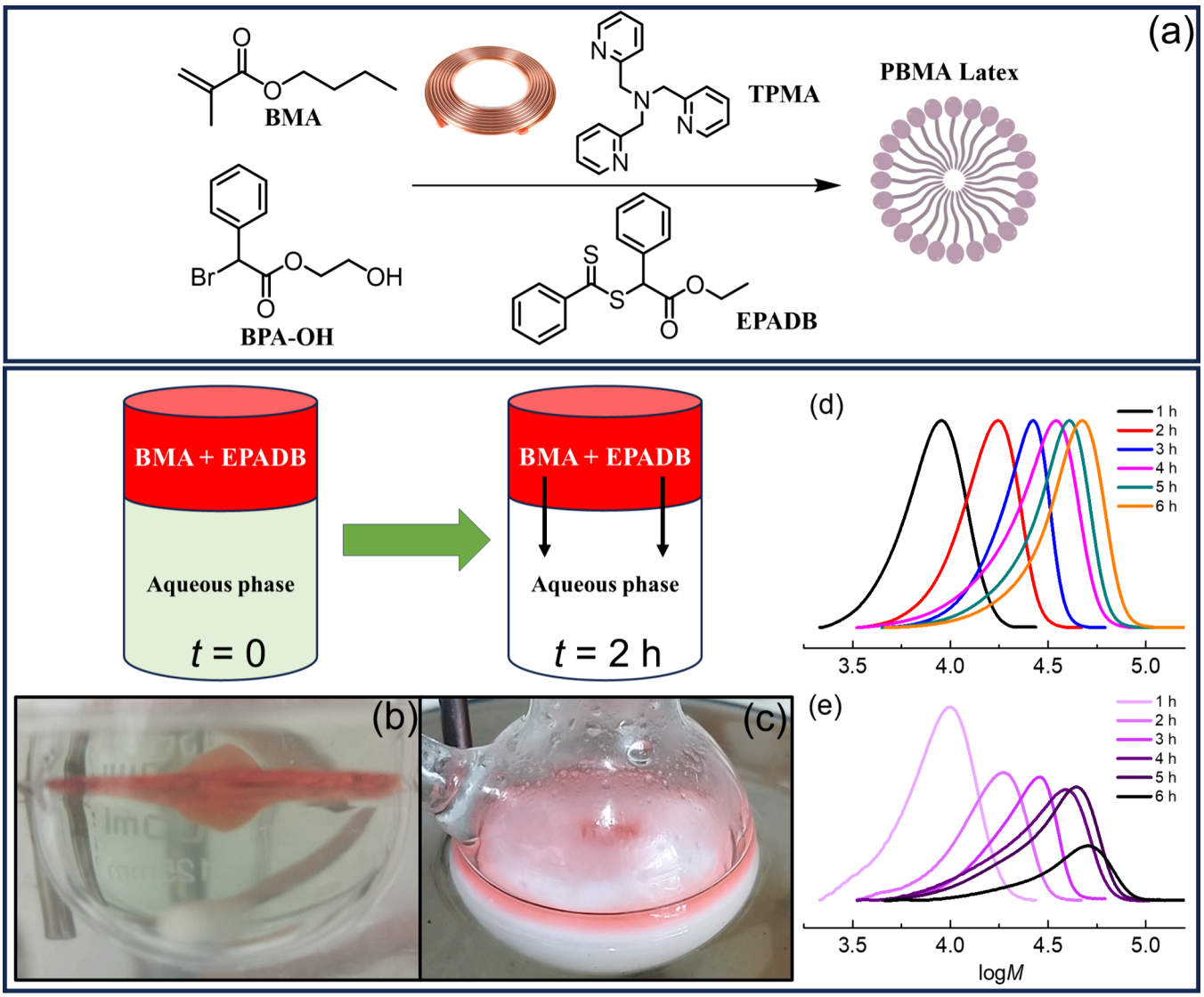

Figure 2. Schematic representation and digital pictures illustrating the concurrent ATRP/DT polymerization of 20 vol % BMA in emulsion: (a) scheme of the reaction; (b) initial state at $t = 0$, where EPADB is fully contained in BMA and floating above the aqueous phase (note the pale green color of the 10^{-3} M $[Cu^{II}TPMA]^{2+}$ catalyst, TPMA = tris(2-pyridylmethyl)amine (L1), contained in the aqueous phase); (c) during polymerization, EPADB diffuses from BMA to engage the radical into concurrent ATRP/DT, causing the aqueous phase to turn pale pink owing to the formation of a stable PBMA latex (the picture was taken after 2 h of reaction); (d) molecular weight distributions of PBMA; and (e) UV chromatograms of PBMA. RI and UV chromatograms are recorded at 1 h intervals; UV chromatograms are normalized against the concentration of PBMA to show the decrease in absorption of the dithiobenzoate chain-end with the increase in the molecular weight of PBMA.

1000 to 0.77 μM, while keeping EPADB constant (C_{BMA}/C_{EPADB} = 314). The lowest Cu loading corresponded to the use of only residual Cu ions in deionized water (0.77 μM, measured by atomic absorption mass spectrometry, AA-MS).

Linear polymerization kinetics were observed for all Cu loadings (Figure 3a-c), with M_n increasing linearly with conversion and low dispersity (Figure 3b). The molecular weight distributions shifted smoothly toward higher MW with conversion (Figure S21). These are unequivocal signs that the ATRP/DT system proceeds via RDRP rather than a free-radical polymerization mechanism. Stable, monodisperse pale-pink latexes were obtained (Figure S26) with a bimodal particle size distribution observed only at low C_{Cu} = 1.44 μM (Figure S26f).

Polymerization was best controlled with 100 μM Cu (Table 1, entry 3). Higher Cu loadings slowed polymerization because of the slow reduction of large amounts of Cu^{II} to Cu^{I} and a higher deactivator concentration. At lower Cu concentrations, the ATRP control decreased, and the combined ATRP/DT process relied more on DT, resulting in a slightly higher dispersity. Acceptable control was retained even at 0.77 μM Cu with the combination of the ATRP/DT mechanism (entry 7, Table 1). This shows the surprising effect of only μM (micromolar) amounts of copper on the polymerization control.

ATRP alone (no EPADB) led to controlled polymerization at 1000 μM Cu; however, the control was poor at 50 μM Cu (entries 9 and 10, Table 1). A comparison of entries 4 and 10 in Table 1 shows the effect of EPADB at a low (50 μM) Cu loading; better control and smaller particle sizes were obtained in the presence of EPADB. A DT-only experiment (RAFT polymerization; Table 1, entry 11) showed poor control, further underscoring the importance of combining ATRP/DT at low Cu loadings.

https://doi.org/10.1021/acs.macromol.4c01812
Macromolecules 2024, 57, 10297−10310

Table 1. ATRP/DT Polymerization of 20 vol % BMA in Emulsion Conditions Modulating C_{Cu} [a]

entry	C_{Cu} (μM)	C_{Cu} (ppm w.r.t. BMA)	t (h)	conv. (%)[b]	$10^{-3} \times M_n^{GPC}$[c]	$10^{-3} \times M_n^{th}$[d]	$Đ$[e]	Z_{ave} (PDI) (nm)[f]	released C_{Cu} (μM)[g]
1	1000	355.6	6	60	34.7	27.3	1.20	121.5 (0.01)	620
2	200	71.1	6	56	21.3	25.4	1.15	142.2 (0.04)	226
3	100	35.5	6	82	30.6	36.9	1.11	100.6 (0.01)	239
4	40	14.2	5	99	39.1	44.8	1.40	86.4 (0.03)	8
5	2	0.71	7	97	60.3	43.4	1.44	42.2 (0.07)	n.d.
6	1.44	0.51	7	89	50.8	40.0	1.45	60.1[j] (0.31)	n.d.
7	0.77[h]	0.26	7	93	64.5	42.4	1.38	39.6 (0.08)	90
8	0.77[i]	0.26	7	90	69.0	40.8	1.70	40.0 (0.12)	0
standalone ATRP and RAFT									
9[k]	1000	355.6	6	75	28.9	34.0	1.30	140.1 (0.06)	n.d.
10[k]	50	18.3	7	93	55.8	41.8	1.75	232.1 (0.07)	n.d.
11[l]	0	0	5	>99	102.9	44.6	2.59	21.5[m] (0.21)	0

[a]General conditions: $C_{BMA}/C_{EPADB}/C_{BPA-OH}/C_{NaBr}$ = 126:0.4:0.4:10, DP = 314, T = 80 °C, $C_{NaBr} = C_{SP}$ = 0.1 M, C_{SDS} = 18.4 wt % BMA, C_{Cu}/C_{TPMA} = 1:2, BMA is used with a HQ inhibitor. n.d. = not determined. [b]Calculated by gravimetry. [c]Calculated by gravimetry: M_n^{th} = conv. × DP × MW_{BMA} + MW_{BPA-OH}. [d]Calculated using THF GPC at T = 30 °C. [e]Calculated from GPC: $Đ = M_w/M_n$. [f]Determined by dynamic light scattering (number distribution, average of three measurements at 20 °C). [g]Determined by AA-MS. [h]Residual Cu ions in deionized water were determined using AA-MS. [i]Residual Cu ions in deionized water and V-501 as the thermal initiator under ICAR conditions (V-501 = 30 mol % of BPA−OH). [j]DLS showed bimodal particle distribution. [k]ATRP without added EPADB chain transfer agent. [l]RAFT polymerization: $C_{BMA}/C_{EPADB}/C_{NaBr}/C_{SP}$ = 126:0.4:10:10, DP = 314, T = 80 °C, $C_{NaBr} = C_{SP}$ = 0.1 M, C_{SDS} = 18.4 wt % BMA, ACVA (4,4'-azobis(4-cyanopentanoic acid)) = 2 mM, BMA is used with HQ inhibitor. [m]DLS revealed a bimodal particle distribution.

AA-MS of the dried latex indicated that a small amount of Cu ions was released from the Cu wire during polymerization (see the last column of Table 1). Similarly, the CV curve at the end of polymerization showed a slight increase in the cathodic current, confirming the release of Cu ions (Figure 1d). This could result from Cu comproportionation (SARA ATRP mechanism), mechanical scrubbing of Cu^0 from the wire, leaching of Cu oxides, or the formation of copper dithiobenzoates or bromides. Scanning electron microscopy revealed that the surface of the wire was slightly worn after 15 polymerization cycles (Figure S32).

One method to regenerate $[Cu^IL]^+$ without increasing the metal load is the thermal decomposition of radical initiator V-501 (Table 1, entry 8 and Figure 4). Under these conditions, polymerization with a dispersity of 1.7 was obtained. The corresponding SARA ATRP (entry 7, Table 1) showed a lower dispersity of 1.38, likely due to the release of additional Cu during the process from the Cu wire.

Quantifying the incorporation of dithiobenzoate end groups into the polymers was challenging because of the continuous diffusion of EPADB into the aqueous phase, which led to an increase in the number of these end groups throughout the reaction. This resulted in poor molecular weight control for RAFT polymerization alone, as the CTA concentration varied over time, preventing effective MW control (Table 1, entry 10). Overall, the contribution of DT to the control of polymer growth appeared to be minor compared with that of ATRP.

Consistent with the predominant role of ATRP in this system, there was good agreement between the experimental M_n^{GPC} and calculated M_n^{th} when considering only the chain initiation of R-Br by ATRP (M_n^{th} = conv. × DP_T × MW_{BMA} + MW_{RBr}, where $DP_T = C_{BMA}/C_{BPA-OH}$ = 314). Table 1 shows M_n^{th} based solely on ATRP initiation without including the contribution of EPADB, owing to the rapid initiation of BPA−OH in the aqueous phase at the start of polymerization. In a simplified scenario, neglecting irreversible radical termination, any deviation of M_n^{GPC} from M_n^{th} (particularly if $M_n^{GPC} < M_n^{th}$) indicates significant radical fragmentation by DT, suggesting the formation of smaller PBMA chains.

The particle size increased with increasing Cu concentration. This might be due to latex destabilization from divalent ions (some $[Cu^{II}TPMA]^{2+}$ might still be present) or to the formation of $[Cu^{II}TPMA\text{-}DS]^+$ complexes that remove the surfactant from the mixture or hamper particle nucleation at high Cu loadings.

2.4. Versatility of ATRP/DT Polymerization: Testing Multiple Amine Ligands. We explored using non-TPMA catalysts for ATRP in emulsion,[51,68,75] which could reduce costs and allow the modulation of catalyst activity by altering the amine ligand structure.[76] We tested nine different Cu catalysts, including challenging ligands like aza-macrocycles and others typically unsuitable for ATRP in emulsion (Scheme 3).[74]

Further electrochemical characterization was performed to understand the affinities of these catalysts for both SP and SDS in micellar environments (see Table S1 in the Supporting Information). First, we observed that all catalysts, except Cu/

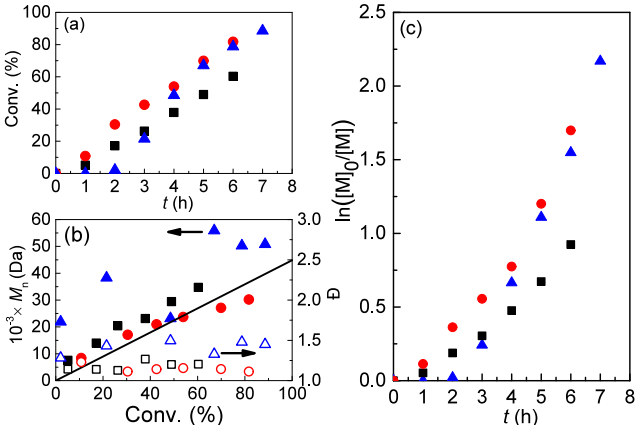

Figure 3. (a) Selected kinetic plots, (b) evolution of M_n and $Đ$ with conversion, and (c) semilogarithmic plots for the concurrent ATRP/DT polymerization of 20 vol % BMA in emulsion at different Cu concentrations, which was initiated by 4 mM BPA−OH in the presence of 0.1 M SP, 0.1 M NaBr, and 1.4 cm Cu^0 wire. Symbols: (■) C_{Cu} = 1000 μM, (●) C_{Cu} = 100 μM, and (▲) C_{Cu} = 1 μM. The reaction conditions are listed in Table 1.

https://doi.org/10.1021/acs.macromol.4c01812
Macromolecules 2024, 57, 10297−10310

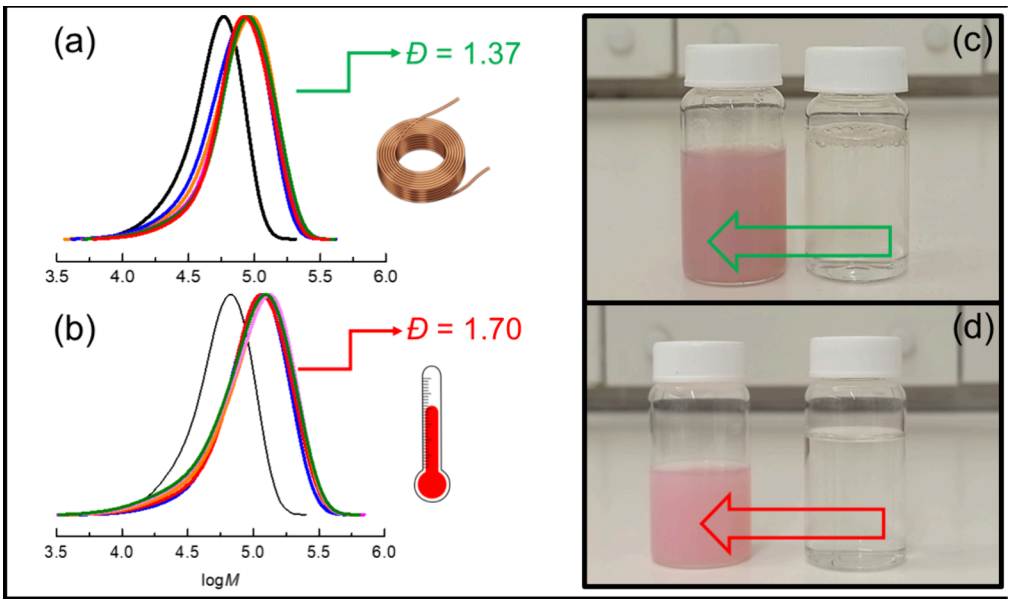

Figure 4. Molecular weight distributions of PBMA produced by concurrent ATRP/DT polymerization in an emulsion using residual Cu in deionized water and regeneration by (a) comproportionation or (b) thermal decomposition of V-501. The chromatograms (RI traces) show the evolution of the molecular weight distribution after each hour of the reaction. Digital images of the aqueous phase at the beginning and end of concurrent ATRP/DT polymerization under emulsion conditions using residual Cu^{II} ions in deionized water employing (c) comproportionation or (d) thermal decomposition of V-501. The latex exhibited a distinct pink color owing to the incorporation of the dithiobenzoate chain end in PBMA.

Table 2. Concurrent ATRP/DT Polymerization of 20 vol % BMA in Emulsion with Different Amine Ligands[a]

entry	ligand	t (h)	conv. (%)[b]	$10^{-3} \times M_n^{app}$,[c]	$10^{-3} \times M_n^{th}$,[d]	$Đ$[e]	Z_{ave} (PDI) (nm)[f]
aryl amines							
1	TPMA (L1)	6	90	38.9	40.6	1.28	121.5 (0.01)
2	TPMA-$(OH)_2$ (L2)	6	88	30.0	39.6	1.19	63.6 (0.12)
3	BPED (L3)	3	94	46.1	42.3	1.44	34.8 (0.04)
alkyl amines							
4	Me_6TREN (L4)	5	98	30.9	44.2	1.20	54.4 (0.02)
5	HMTETA (L5)	5	83	37.3	37.8	1.34	89.5[g] (0.49)
6	PMDETA (L6)	5	85	37.0	38.5	1.44	67.9 (0.41)
7	TREN (L7)	6	91	119.1	41.3	1.37	42.7 (0.18)
macrocyclic amines							
8	Me_4Cyclam (L8)	6	87	169.8	39.4	1.47	38.2 (0.07)
9	*meso*-Me_6Cyclam (L9)	6	85	84.1	38.5	1.28	78.5[g] (0.41)

[a]General conditions: $C_{BMA}/C_{Cu}/C_L/C_{NaBr}/C_{HEBiB}/C_{EPADB}$ = 126:0.1:0.2:10:0.4:0.4, DP = 314, T = 80 °C, $C_{Cu} = 10^{-3}$ M, $C_{NaBr} = C_{SP}$ = 0.1 M, C_{SDS} = 18.4 wt %, BMA is used with a HQ inhibitor. [b]Calculated by gravimetry. [c]Calculated by gravimetry: M_n^{th} = conv. × DP × MW_{BMA} + MW_{HEBiB}. [d]Calculated using THF GPC at T = 30 °C. [e]Calculated from GPC: $Đ = M_w/M_n$. [f]Determined by dynamic light scattering (number distribution, average of three measurements at 20 °C). [g]DLS revealed a bimodal particle distribution.

TREN, showed a slight shift toward negative potentials upon the addition of SP. This suggests that the deactivator was weakly coordinated to the pyruvate anion in most of the catalysts. Cu complexes with TPMA (L1), TPMA-$(OH)_2$ (L2), Me_6TREN (L4), PMDETA (L6), and TREN (L7) preferentially bonded with SDS in their Cu^{II} oxidation state, while those with BPED (L3) and HMTETA (L5) preferentially bonded with SDS in their Cu^{I} state. Among the tested catalysts, Cu^{II}/BPED (L3) exhibited the lowest affinity for anionic micelles, whereas Cu^{II}/TPMA-$(OH)_2$ exhibited the highest affinity. This ligand (see section S3.1.1 of the Supporting Information) has two of its three rings modified by a strong electron-donating group (*N*-methylaminoethanol). *para*-Substitution enhances the electronic density at the metal center by stabilizing the Cu^{II} oxidation state and increasing k_{act}.[21,74,77] The pendent hydroxyl groups instead increase the micellar affinity. The results of this series of polymerizations using the different catalysts are presented in Table 2.

The ATRP/DT concurrent mechanisms of radical taming enabled polymerization with all catalysts, including Cu/TREN (L7) and Cu/aza-macrocycles (L8−9). In these cases, M_n^{app} differed from M_n^{th}, likely because of exacerbated radical generation in water at the beginning of polymerization. We observed $Đ < 1.5$, regardless of the affinity of the Cu catalysts for the micelles.

The results shown in Table 2 deviate from those of traditional solvent-based ATRP, which typically depends on the ability of the catalyst to activate C−Br bonds. The compartmentalized emulsion environment adds complexity to the behavior of each catalyst. Cu/BPED, which had the lowest micelle affinity, led to faster polymerization. In contrast, Cu/Me_6TREN- and Cu/TPMA-based catalysts, with higher micelle affinities, resulted in slower but better-controlled polymerization owing to tighter

https://doi.org/10.1021/acs.macromol.4c01812
Macromolecules 2024, 57, 10297−10310

Table 3. Comparison of Concurrent ATRP/DT Polymerization of 20 vol % BMA in Emulsion Using Comproportionation or Regeneration by Thermal Decomposition with Different Initiators[a]

entry	mechanism	agent	t (h)	conv. (%)[b]	$10^{-3} \times M_n^{app}$,[c]	$10^{-3} \times M_n^{th}$,[d]	$Đ$[e]	Z_{ave} (PDI) (nm)[f]	zeta potential (mV)
using RBr = BPA−OH									
1	ATRP/DT	Cu^0	6	60	34.7	27.3	1.20	121.5 (0.01)	−77
using RBr = HEBiB									
2	ATRP/DT	Cu^0	6	90	38.9	40.6	1.28	71.7 (0.01)	−77
3	ATRP	Cu^0	6	16	9.8	7.2	1.86	109.8 (0.19)	−50
4[g]	ATRP/DT	V-501	6	94	31.7	42.3	1.15	139.8[h] (0.03)	−62
5	ATRP/DT	applied current	5	72	33.4	32.6	1.08	43.3 (0.20)	−80
using RBr = HEBrP and HEBrAc									
6	ATRP/DT	Cu^0	7	87	37.1	39.1	1.44	42.1 (0.30)	−105
7	ATRP	Cu^0	6	22	28.9	10.3	1.85	78.8 (0.06)	n.d.
8	ATRP/DT	Cu^0	7	78	84.2	35.0	1.50	41.0 (0.07)	−97
9	ATRP	Cu^0	6	0				n.d.	n.d.

[a]General conditions: $C_{BMA}/C_{Cu}/C_{TPMA}/C_{NaBr}/C_{RBr}/C_{EPADB}$ = 126:0.1:0.2:10:0.4:0.4, T = 80 °C, except for entry 4, where T = 75 °C and C_{SDS} = 18.4 wt % BMA. BMA is used with a HQ inhibitor. n.d. = not determined. [b]Calculated by gravimetry. [c]Calculated by gravimetry: M_n^{th} = conv. × DP × MW_{BMA} + MW_{RBr}. [d]Calculated using THF GPC at T = 30 °C. [e]Calculated from GPC: $Đ = M_w/M_n$. [f]Determined by dynamic light scattering (number distribution, average of three measurements at 20 °C). [g]Using V-501 conventional initiator: $C_{V\text{-}501}$ = 30% × C_{HEBiB}. [h]3% aggregates with Z_{ave} > 5000 nm.

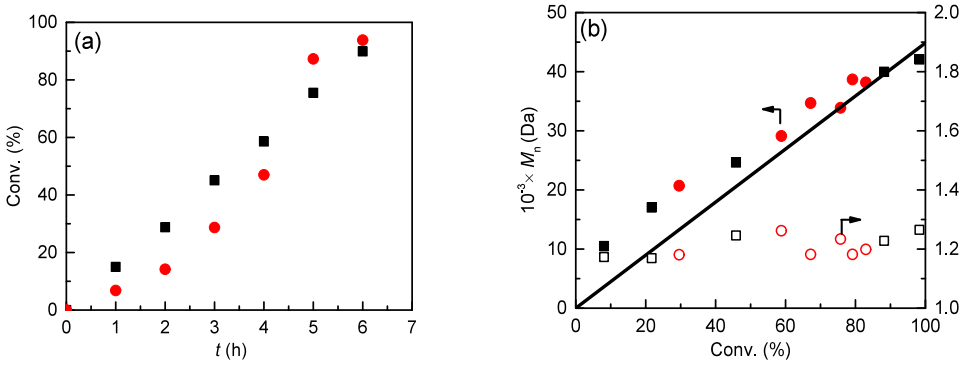

Figure 5. (a) Kinetic plots and (b) evolution of M_n and $Đ$ with conversion for the concurrent ATRP/DT polymerization of 20 vol % BMA in emulsion conditions, which was initiated by 4 mM HEBiB in the presence of 0.1 M SP and 0.1 M NaBr. Symbols: (■) 1.4 cm Cu^0 wire, (●) V-501 thermal initiator. The filled symbols refer to the left ordinate, and the empty symbols refer to the right ordinate.

control at the polymerization locus. Despite being less active in ATRP, ligands such as PMDETA (L6), BPED (L3), and HMTETA (L5) quickly achieved controlled PBMA with high monomer conversion. The latexes remained stable (Figure S28 and Table S6); however, those from Cu/L5 and Cu/L9 showed bimodal particle size distributions, and the Cu/L7 latex had less than 3% aggregates with Z_{ave} > 5000 nm.

Next, we explored different ATRP initiators (Table 3). The use of 2-hydroxyethyl α-bromoisobutyrate (HEBiB) instead of BPA−OH offers three advantages: (i) higher conversion, (ii) better molecular weight control, and (iii) commercial availability or easy synthesis. BPA−OH showed too-high reactivity with Cu complexes, which led to biradical termination, slower polymerization, and increased molecular weight. Inexpensive and well-behaving HEBiB is crucial for the scale-up of ATRP/DT polymerization of PBMA in emulsions. Unlike the behavior observed for the BPA−OH initiator (cfr. Table 1, entries 4 and 10), the ATRP/DT method with the HEBiB initiator improved the conversion and $Đ$ compared to the control ATRP alone (without DT, Table 3, entries 2 and 3), due to combined radical taming by both mechanisms.

Next, we compared the modes of regeneration of $[Cu^IL]^+$. Comporportionation, thermal initiation (V-501), and alternating current electrolysis (square wave of I_{app} = ± 24 μA at 0.15 Hz) led to similar polymerization rates and controls (Table 3, entries 2, 4, and 5), indicating the versatility of the ATRP/DT polymerization method for various techniques, including external stimuli, among which the electrochemical method yielded the lowest $Đ$. We also tested the secondary initiator 2-hydroxyethyl 2-bromopropionate (HEBrP, Table 3 entries 6 and 7) and primary 2-hydroxyethyl 2-bromoacetate (HEBrAc, Table 3 entry 8 and 9). ATRP/DT polymerization can also be initiated (although with some limitations) by initiators that generate secondary and primary initiating radicals. Unsurprisingly, the corresponding control ATRPs (without DT) were indeed ill-defined polymerizations, and the ATRP initiated by HEBrAc did not start. This was due to the mismatched reactivity of the secondary and primary initiating radicals with the tertiary radicals formed after the first addition of BMA. The reactivity of tertiary alkyl halides is much higher than that of secondary alkyl halides due to better stabilization of the radicals derived from the former species and a lower C−Br bond dissociation energy.[78] This is also in line with earlier results on the "penultimate effect", which is especially important for methacrylates, as they are very sensitive to the structure of the penultimate unit.

Selected conversion plots and the evolution of M_n^{app} and $Đ$ vs conversion are shown in Figure 5. All PBMA latexes were stable and showed a monomodal particle size distribution (Figure S29

https://doi.org/10.1021/acs.macromol.4c01812
Macromolecules 2024, 57, 10297−10310

and Table S6) and <3% aggregates with Z_{ave} > 5000 nm when V-501 was used (Table 3, entry 4 and Figure S29d). The zeta potentials of our latexes were between −50 and −80 mV, indicating moderate-to-excellent colloidal stability.

2.5. Chain Extension and Synthesis of Functional Polymers. We confirmed the retention of the chain-end functionality by conducting chain extension *in situ* using two PBMA macroinitiators after the addition of fresh BMA at 1 mM (Figure 6a) and 50 μM (Figure 6b) concentrations of the catalyst in the presence of a Cu^0 wire. ^{1}H NMR confirmed the presence of the dithiobenzoate chain end (Figure S37). In both cases, there was evidence of a living macroinitiator. The UV detector at 310 nm indicated that the PBMA-DB chains were living and shifted to a higher MW. The UV detector exclusively detected PBMA-DB because PBMA-Br did not absorb light at that wavelength. Notably, the RI traces (sensitive to the entire PBMA sample) and UV traces (selective for PBMA-DB chains) shifted simultaneously during the chain extension experiments. The slight difference between the RI and UV traces likely stems from the loss of the CTA chain-end functionality during polymerization. The main distinction is visible in Figure 6b for the block copolymer made with the 50 ppm catalyst, where the UV signal is shifted to higher molecular weights. This suggests that some low-molecular-weight chains terminated at the end of the chain extension, whereas most high-molecular-weight chains retained the CTA functionality. An additional chain extension by thermal RAFT, in which only the C−DB chain end was activated and not the C−Br end, also confirmed the livingness of PBMA-DB (Figure 6c), resulting in an expected bimodal molecular weight distribution.

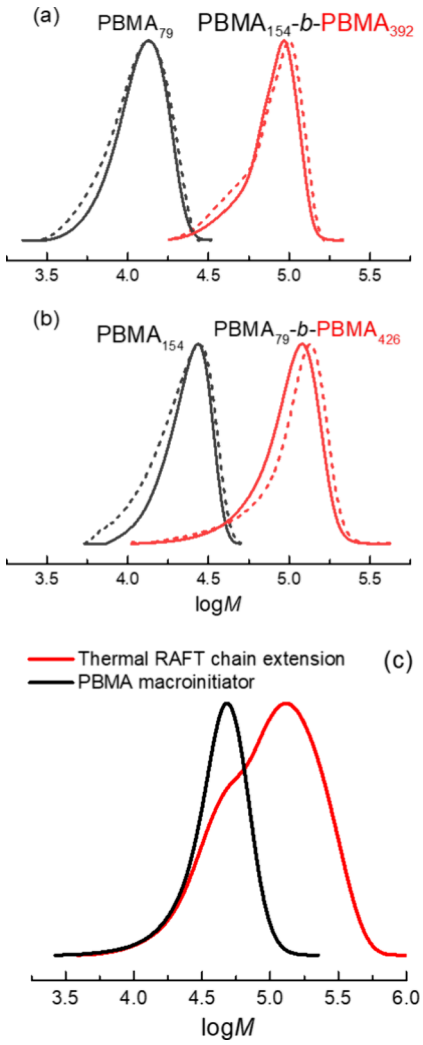

Figure 6. Molecular weight distributions of the macroinitiator and diblock homopolymer obtained during chain extension. The solid line represents the refractive index detector, and the dashed line represents the UV detector set at 310 nm. (a) 1 mM Cu catalyst: $PBMA_{79}$ (black line) and $PBMA_{79}$-*b*-$PBMA_{426}$ (red line) homopolymers. The $PBMA_{79}$ macroinitiator had the following properties: M_n = 11200, $Đ$ = 1.13, and conv. BMA = 47.5%; $PBMA_{79}$-*b*-$PBMA_{426}$ had M_n = 72000, $Đ$ = 1.15, and conv. BMA = 33.3%. (b) 50 μM Cu catalyst: $PBMA_{154}$ (black line) and $PBMA_{154}$-*b*-$PBMA_{392}$ (red line) homopolymers. The $PBMA_{154}$ macroinitiator had M_n = 21900, $Đ$ = 1.10, and conv. BMA = 71.1%; $PBMA_{154}$-*b*-$PBMA_{392}$ had M_n = 77900, $Đ$ = 1.21, and conv. BMA = 74.9%. (c) Chain extension of the PBMA macroinitiator (M_n = 44500, $Đ$ = 1.21) by thermal RAFT.

Additionally, the ATRP/DT emulsion procedure using only 20 μM Cu was compatible with the incorporation of functional methacrylate monomers (Figures S34−36). The first copolymer was prepared using the fluorescent comonomer 7-(2-methacryloyloxyethoxy)coumarin (CouMMA) with 1 mol % BMA.[79] The second copolymer was obtained using *N*-phthalimidyl methacrylate (PhthMMA) as a comonomer with 5 mol % BMA. PhthMMA contains a phthalimide, which under specific conditions can serve as a starting point for backbone depolymerization.[80−83] Successful incorporation of the functional monomers was monitored by fluorescence (Figure S36).

2.6. Scale-Up of ATRP/DT Polymerization to 1 L. For scale-up, we prioritized an approach that minimized reagent demand, especially SDS load and cost (section S5 of the Supporting Information). We determined that 4.6 wt % SDS was more suitable for scales larger than 18.4 wt % (see Table S5 in section S10 of the Supporting Information). Therefore, we further optimized at a small scale (20 mL) the reactions requiring less than 100 μM catalyst and used 4.6 wt % SDS, with a C_{HEBiB}/C_{EPADB} ratio of 2:1 (Table 4). Selected conversion plots and the evolution of M_n^{app} and $Đ$ vs conversion, indicating a well-behaved RDRP under these conditions, are shown in Figure S33.

The most suitable conditions for quantitative conversion and the lowest $Đ$ were found at C_{Cu} = 50 μM (18.3 ppm with respect to BMA) (Table 4, entry 4). The optimized reaction (Table 4, entry 4) was scaled up to 80 mL and then to 1 L (scale-up factors of 4 and 50, respectively; Table 4, entries 6 and 7, Figure 7, and Figure S25). The choice of reactor depended on the reaction volume; Schlenk reactors were used for small scales (20−80 mL), whereas a cylindrical SS304 reactor was used for the 1 L scale (Table S4). Experimentally, it was ensured that the BMA remained separated from the aqueous phase during the entire reaction to avoid excessive turbulence caused by overstirring. We observed nearly quantitative conversions at 20 and 80 mL, with $Đ$ values ranging from 1.21 to 1.23, and M_n^{app} showed good agreement with M_n^{th}. At the 1 L scale, the polymerization slowed, reaching 82% after 6 h. $Đ$ remained unchanged at 1.20, and M_n^{app} aligned well with M_n^{th} (determined for ATRP activation alone). The particle size increased only slightly during polymerization, indicating that latex was relatively stable after the nucleation stage (Figure 7c). All latexes remained stable over time and exhibited a monomodal particle size distribution (Figures S30 and S31). Zeta potentials in the negative −80 to −100 mV range further reinforced the remarkable colloidal stability of these latexes.

https://doi.org/10.1021/acs.macromol.4c01812
Macromolecules 2024, 57, 10297−10310

Table 4. Concurrent ATRP/DT Polymerization and Standalone ATRP or RAFT of 20 vol % BMA in Emulsion at T = 75 °C[a]

entry	C_{Cu} (μM)	C_{Cu} (ppm w.r.t. BMA)	t (h)	conv. (%)[b]	$10^{-3} \times M_n^{app,c}$	$10^{-3} \times M_n^{th,d}$	$Đ^e$	zeta potential (mV)[f]	Z_{ave} (PDI) (nm)[g]	Theoretical E-factor[h] with H_2O	Theoretical E-factor[h] without H_2O
concurrent ATRP/DT polymerization											
1	5	1.78	10	83	50.6	37.5	1.51	−86	116.5 (0.12)	19.5	10.6
2	10	3.55	7	87	49.1	39.3	1.43	−76	111.1 (0.10)	16.2	7.8
3	25	9.15	6	94	46.2	42.3	1.29	−70	160.5 (0.02)	11.2	3.4
4	50	18.3	6	>99	47.5	44.8	1.23	−64	131.4 (0.02)	8.1	0.68
5	100	35.5	8	68	35.5	30.7	1.23	−82	139.8 (0.03)	35.0	24.2
scale-up											
6[i]	50	18.3	6	>99	47.5	44.8	1.23	−102	115.7 (0.01)	5.7	0.44
7[j]	50	18.3	5	98	44.5	44.3	1.21	−92	104.9 (0.03)	6.0	0.61

[a]General conditions: C_{BMA} = 1.26 M, C_{Cu}/C_{TPMA} = 1:2. C_{HEBiB}/C_{EPADB} = 2:1. C_{SDS} = 4.6 wt % BMA. [b]Calculated by gravimetry. [c]Calculated by gravimetry: M_n^{th} = conv. × DP × MW_{BMA} + MW_{HEBiB}. [d]Calculated from THF GPC at T = 30 °C. [e]Calculated from GPC: $Đ = M_w/M_n$. [f]Determined by dynamic light scattering (number distribution, average of three measurements at 20 °C). [g]Average of three measurements at 20 °C [h]Calculated without purifying PBMA. [i]Reaction of 80 mL. [j]Reaction of 1 L.

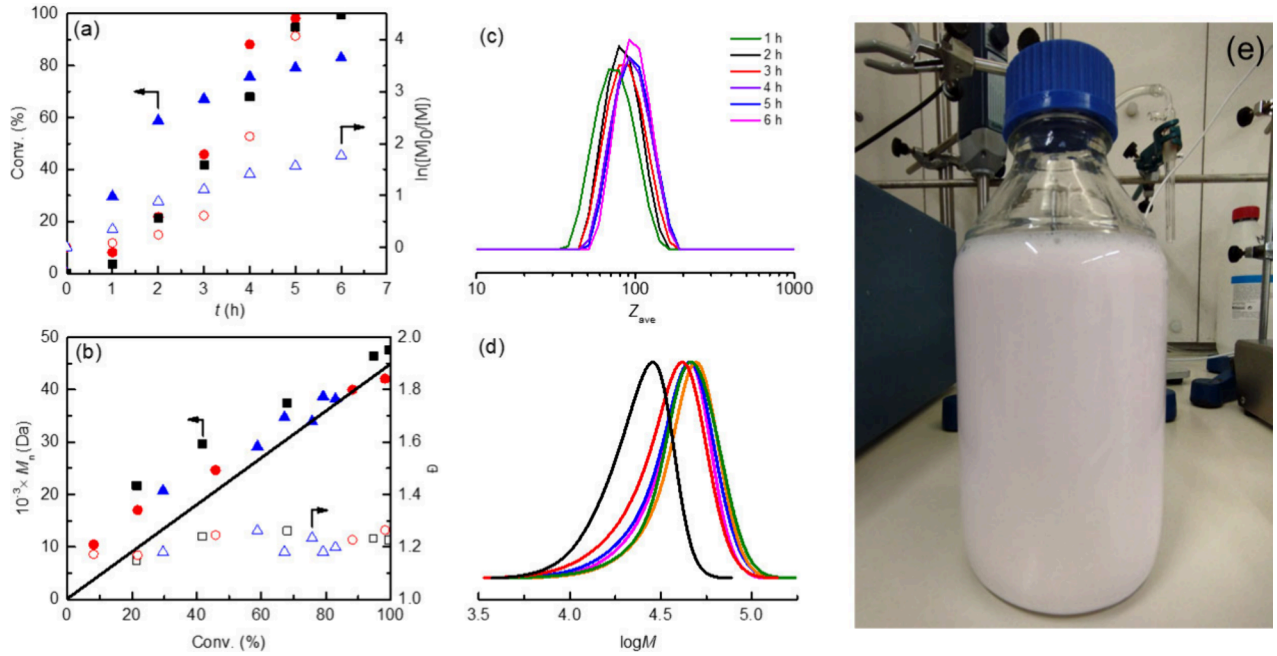

Figure 7. (a) Conversion and semilogarithmic plots, (b) evolution of M_n and $Đ$ with conversion, (c) intensity evolution of Z_{ave} with time, and (d) evolution of the macromolecular weight distribution of the emulsion concurrent ATRP/DT polymerization of 20 vol % BMA, which was initiated by 4 mM HEBiB in the presence of 0.1 M SP and 0.1 M NaBr at 1 L scale. (e) Picture of the recovered pale pink stable latex of PBMA at the end of the reaction, the glass bottle has a nominal capacity of 1 L. Symbols: (■) V_f = 20 mL, (●) V_f = 80 mL, (▲) V_f = 1000 mL.

Our cost analysis (Tables S2 and S3) indicated that PBMA synthesized at a 1 L scale was approximately twice as cost-effective as in previous reports,[59] even with the relatively high cost of EPADB at ∼26 €/g. Although EPADB is cheaper than many dithioesters, its cost is affected by the high cost of the EBPA precursor (Tables S2 and S3). Future cost reductions could come from increasing the polymerization volume and solid content, reducing EPADB (and EBPA) costs, or using less expensive dithioesters.

We calculated two theoretical E-factors (E-factor = mass of waste/mass of product), one where water was considered as waste like other substances and another where water, sodium pyruvate, and phosphate salts were excluded from the waste. The acceptable E-factors are 1−5 for bulk chemicals and <500 for fine chemicals. Scaling from 0.02 to 1 L, our E-factor with water as waste dropped from 8.14 to 5.71. Excluding water and nonharmful reagents, the E-factor ranged from 0.445 to 0.684, indicating that ATRP/DT polymerization in emulsion is more environmentally friendly than that in solution or miniemulsion.[63]

2.8. Dithiobenzoate End-Group Removal Exploiting ORR. To address the pink color of the latex caused by dithiobenzoate end groups, we explored methods for end-group removal. This color removal is crucial for coating and optoelectronic applications and essential for reducing the cytotoxicity of CTA residues in biologically related materials.[84] Various techniques, including the use of H_2O_2, have been investigated for removing RAFT end-groups.[85]

Here, we propose an advanced method involving a Cu-catalyzed ORR process to generate H_2O_2 *in situ* using the same ATRP catalyst.[86,87] H_2O_2 then reacts with sodium pyruvate or facilitates radical-induced oxidation of the dithiobenzoate end group, resulting in OH-capped PBMA (Figure 8).

https://doi.org/10.1021/acs.macromol.4c01812
Macromolecules 2024, 57, 10297−10310

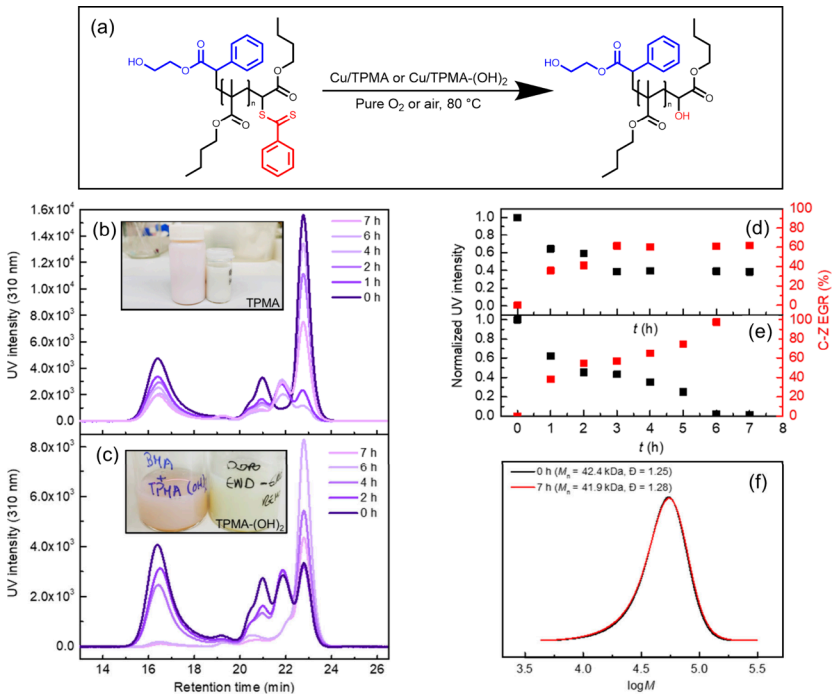

Figure 8. (a) Radical-induced oxidation of PBMA-DB using H_2O_2. The generated H_2O_2 produced by the ORR cleaves the dithiobenzoate end group via radical-induced oxidation. UV GPC chromatograms recorded during end-group removal by ORR with (b) atmospheric O_2 or (c) pure O_2; $C_{[CuIITPMA]2+}$ = 50 μM, T = 80 °C. The insets show digital pictures of the corresponding latexes before and after end-group removal. (d) Kinetics of end-group removal (C-Z EGR) with (d) atmospheric O_2 or (e) pure O_2. The black squares (■) refer to the normalized UV signal intensity, whereas the red squares (■) refer to the % of end-group removal. (f) Molecular weight distribution of PBMA at the beginning (black line, Z_{ave} = 114.9 nm) and after (red line, Z_{ave} = 125.5 nm) end-group removal using pure O_2.

By simply supplying oxygen to the reaction headspace at the end of polymerization, the end group was removed, as evidenced by UV-GPC with the detector set at 310 nm. Our experiments demonstrated that both atmospheric O_2 and pure O_2 are suitable for generating OH-capped PBMA[85] (Figure 8a and b). Specifically, using 50 μM $[Cu^{II}TPMA]^{2+}$ at T = 80 °C, approximately 61% of the end-groups were cleaved after 7 h under atmospheric O_2 conditions, whereas nearly 98% were cleaved when pure O_2 was used (see the calculation in eq S6). This noninvasive method offers several advantages: it does not require the destruction of the emulsion and does not significantly change the particle size or other properties of the latex (with only a 1.2% change in M_n, 2.3% change in $Đ$, and 8.4% change in Z_{ave}, as shown in Figure 8c–e).[88] Additionally, it is safer than adding concentrated H_2O_2, followed by quenching. The slight change in Z_{ave} (10.6 nm) could be due to aggregation or changes in the surface properties of the PBMA particles. During end-group removal, the mixture was stirred at 600 rpm, exerting a much higher shear force to promote the diffusion of O_2 into the emulsion and its reduction to H_2O_2 by the Cu catalyst.

The pH of the emulsion changed during chain-end removal; the ORR consumed two protons to produce H_2O_2 from O_2 supplied by the phosphate buffer at pH 5.0, until the buffer was consumed and more protons were supplied by water. At the end of the removal process, the pH was 7.59. This may also influence the particle size distribution and Z_{ave}. The remarkable colloidal stability of the emulsion was preserved (the zeta potential after end-group removal was just 4 mV higher, −88.6 mV). A comparison between the initial pale pink and final white latexes is shown in the insets of Figure 8b and c.

In addition to using $[Cu^{II}TPMA]^{2+}$, we also found that the catalyst $[Cu^{II}TPMA\text{-}(OH)_2]^{2+}$ achieved similar end-group removal efficacy, with approximately 99% cleavage achieved using pure O_2 over a 7 h period.

Although this method is advantageous for the final application, it results in the loss of livingness of PBMA capped with dithobenzoate. After the postpolymerization process, PBMA consists of a mixture of −OH and −Br terminated chains, and H_2O_2 can induce reactions that compromise the living nature of the polymer.

3. CONCLUSIONS

We developed a concurrent ATRP/DT polymerization process in an emulsion using nine different catalysts at extremely low concentrations. This method integrates the mechanistic aspects of both ATRP and DT polymerization, allowing precise control of propagating radicals. Despite the common belief that these mechanisms are distinct, our work shows that they can coexist in emulsions, creating a synergistic effect that surpasses the performance of each mechanism alone. This dual approach resolves the limitations faced by the single ATRP and RAFT processes in emulsion systems. DT polymerization allowed the use of a broader range of amine ligands, facilitated scale-up with a commercially available initiator, and reduced the amount of Cu catalyst required without compromising polymerization control. We successfully scaled up the ATRP/DT emulsion polymerization of BMA to a 1 L scale using thermal initiator V-501 with only 50 μM Cu. We demonstrated the livingness of PBMA capped with either bromide or dithiobenzoate groups by creating well-defined block copolymers and synthesized functionalized PBMA statistical copolymers with fluorescent comonomers, demonstrating their potential applications. The

https://doi.org/10.1021/acs.macromol.4c01812
Macromolecules 2024, 57, 10297−10310

dithiobenzoate end-groups were selectively removed using *in situ* generated H_2O_2 from the same ATRP catalyst via ORR by supplying air to the reactor.

Our work emphasizes the environmental benefits of ATRP/DT polymerization, as demonstrated by its low *E*-factor, and presents it as a novel and sustainable RDRP method for emulsions, advancing beyond the traditional limitations of ATRP and RAFT polymerization.

■ ASSOCIATED CONTENT

Supporting Information

The Supporting Information is available free of charge at https://pubs.acs.org/doi/10.1021/acs.macromol.4c01812.

Additional experimental details, materials, procedures for reagent synthesis, equipment, supplemental characterizations (including electrochemical), cost analysis, recorded molecular weight distributions, recorded DLS distributions, additional reactor details, SEM images, copolymer characterization, and supporting references (PDF)

■ AUTHOR INFORMATION

Corresponding Author

Francesco De Bon − *Centre for Mechanical Engineering Materials and Processes (CEMMPRE), ARISE, Department of Chemical Engineering, University of Coimbra, 3030-790 Coimbra, Portugal;* orcid.org/0000-0003-1858-3390; Email: francesco@eq uc.pt

Authors

Teresa J. Lourenço Bernardino − *Centre for Mechanical Engineering Materials and Processes (CEMMPRE), ARISE, Department of Chemical Engineering, University of Coimbra, 3030-790 Coimbra, Portugal*

Arménio Coimbra Serra − *Centre for Mechanical Engineering Materials and Processes (CEMMPRE), ARISE, Department of Chemical Engineering, University of Coimbra, 3030-790 Coimbra, Portugal*

Marco Fantin − *Department of Chemical Sciences, University of Padova, 35131 Padova, Italy;* orcid.org/0000-0001-9581-2076

Krzysztof Matyjaszewski − *Department of Chemistry, Carnegie Mellon University, Pittsburgh, Pennsylvania 15213, United States;* orcid.org/0000-0003-1960-3402

Jorge Fernando Jordao Coelho − *Centre for Mechanical Engineering Materials and Processes (CEMMPRE), ARISE, Department of Chemical Engineering, University of Coimbra, 3030-790 Coimbra, Portugal; IPN, Instituto Pedro Nunes, Associação para a Inovação e Desenvolvimento em Ciência e Tecnologia, 3030-199 Coimbra, Portugal;* orcid.org/0000-0001-9351-1704

Complete contact information is available at: https://pubs.acs.org/10.1021/acs.macromol.4c01812

Author Contributions

F.D.B. conceived the work, designed the experiments, and drafted the initial manuscript. F.D.B. and T.L.B. performed the experiments and analyzed the data. J.F.J.C. and F.D.B. supervised this work. F.D.B. and J.F.J.C. acquired funding. All authors discussed the results and contributed to the preparation and editing of the manuscript. All authors have agreed to the final version of the manuscript.

Notes

The authors declare no competing financial interest.

■ ACKNOWLEDGMENTS

F.D.B. and T.L.B. thank FCT for the PTDC/EQU-EQU/2686/2020 project (POLYELECTRON). F.M. acknowledges PRIN 2022 "Biocommon" - CUP C53D23004400006. The NMR data were obtained at the Nuclear Magnetic Resonance Laboratory of the Coimbra Chemistry Centre (http://www.nmrccc.uc.pt), University of Coimbra, supported in part by Grant REEQ/481/QUI/2006 from FCT, POCI-2010, and FEDER, Portugal. This research was partially sponsored by FEDER funds through the program COMPETE (Programa Operacional Factores de Competitividade) and by national funds through FCT (Fundação para a Ciência e a Tecnologia) under the projects UIDB/00285/2020 and LA/P/0012/2020. K.M. acknowledges support from NSF (CHE 2401112).

■ REFERENCES

(1) Corrigan, N.; Jung, K.; Moad, G.; Hawker, C. J.; Matyjaszewski, K.; Boyer, C. Reversible-deactivation radical polymerization (Controlled/living radical polymerization): From discovery to materials design and applications. *Prog. Polym. Sci.* **2020**, *111*, 101311.

(2) Pan, X.; Fantin, M.; Yuan, F.; Matyjaszewski, K. Externally controlled atom transfer radical polymerization. *Chem. Soc. Rev.* **2018**, *47* (14), 5457−5490.

(3) Matyjaszewski, K. Advanced Materials by Atom Transfer Radical Polymerization. *Adv. Mater.* **2018**, *30* (23), No. e1706441.

(4) Nothling, M. D.; Fu, Q.; Reyhani, A.; Allison-Logan, S.; Jung, K.; Zhu, J.; Kamigaito, M.; Boyer, C.; Qiao, G. G. Progress and Perspectives Beyond Traditional RAFT Polymerization. *Advanced Science* **2020**, *7* (20), 2001656.

(5) Destarac, M. Controlled Radical Polymerization: Industrial Stakes, Obstacles and Achievements. *Macromol. React. Eng.* **2010**, *4* (3−4), 165−179.

(6) Destarac, M. Industrial development of reversible-deactivation radical polymerization: is the induction period over? *Polym. Chem.* **2018**, *9* (40), 4947−4967.

(7) Matyjaszewski, K.; Spanswick, J. Controlled/living radical polymerization. *Mater. Today* **2005**, *8* (3), 26−33.

(8) Baker, S. L.; Kaupbayeva, B.; Lathwal, S.; Das, S. R.; Russell, A. J.; Matyjaszewski, K. Atom Transfer Radical Polymerization for Biorelated Hybrid Materials. *Biomacromolecules* **2019**, *20* (12), 4272−4298.

(9) Matyjaszewski, K.; Tsarevsky, N. V. Macromolecular engineering by atom transfer radical polymerization. *J. Am. Chem. Soc.* **2014**, *136* (18), 6513−33.

(10) Matyjaszewski, K.; Tsarevsky, N. V. Nanostructured functional materials prepared by atom transfer radical polymerization. *Nat. Chem.* **2009**, *1* (4), 276−88.

(11) Tsarevsky, N. V.; Matyjaszewski, K. "Green" atom transfer radical polymerization: from process design to preparation of well-defined environmentally friendly polymeric materials. *Chem. Rev.* **2007**, *107* (6), 2270−99.

(12) Matyjaszewski, K.; Xia, J. Atom transfer radical polymerization. *Chem. Rev.* **2001**, *101* (9), 2921−90.

(13) Wang, J.-S.; Matyjaszewski, K. Controlled/"living" radical polymerization. atom transfer radical polymerization in the presence of transition-metal complexes. *J. Am. Chem. Soc.* **1995**, *117* (20), 5614−5615.

(14) Allegrezza, M. L.; Konkolewicz, D. PET-RAFT Polymerization: Mechanistic Perspectives for Future Materials. *ACS Macro Lett.* **2021**, *10* (4), 433−446.

(15) Tian, X.; Ding, J.; Zhang, B.; Qiu, F.; Zhuang, X.; Chen, Y. Recent Advances in RAFT Polymerization: Novel Initiation Mechanisms and Optoelectronic Applications. *Polymers* **2018**, *10* (3), 318.

(16) Perrier, S. 50th Anniversary Perspective: RAFT Polymerization—A User Guide. *Macromolecules* **2017**, *50* (19), 7433−7447.

(17) Moad, G.; Rizzardo, E.; Thang, S. H. RAFT Polymerization and Some of its Applications. *Chemistry - An Asian Journal* **2013**, *8* (8), 1634−1644.
(18) Boyer, C.; Bulmus, V.; Davis, T. P.; Ladmiral, V.; Liu, J.; Perrier, S. Bioapplications of RAFT Polymerization. *Chem. Rev.* **2009**, *109* (11), 5402−5436.
(19) Truong, N. P.; Jones, G. R.; Bradford, K. G. E.; Konkolewicz, D.; Anastasaki, A. A comparison of RAFT and ATRP methods for controlled radical polymerization. *Nat. Rev. Chem.* **2021**, *5* (12), 859−869.
(20) Lorandi, F.; Fantin, M.; Matyjaszewski, K. Atom Transfer Radical Polymerization: A Mechanistic Perspective. *J. Am. Chem. Soc.* **2022**, *144*, 15413.
(21) Lorandi, F.; Matyjaszewski, K. Why Do We Need More Active ATRP Catalysts? *Isr. J. Chem.* **2020**, *60* (1−2), 108−123.
(22) Lanzalaco, S.; Fantin, M.; Scialdone, O.; Galia, A.; Isse, A. A.; Gennaro, A.; Matyjaszewski, K. Atom Transfer Radical Polymerization with Different Halides (F, Cl, Br, and I): Is the Process "Living" in the Presence of Fluorinated Initiators? *Macromolecules* **2017**, *50* (1), 192−202.
(23) Li, M.; Wang, S.; Li, F.; Zhou, L.; Lei, L. Iodine-mediated photo-controlled atom transfer radical polymerization (photo-ATRP) and block polymerization combined with ring-opening polymerization (ROP) via a superbase. *Polym. Chem.* **2020**, *11* (41), 6591−6598.
(24) Parkatzidis, K.; de Haro Amez, L.; Truong, N. P.; Anastasaki, A. Cu(0)-RDRP of acrylates using an alkyl iodide initiator. *Polym. Chem.* **2023**, *14* (14), 1639−1645.
(25) Nicolaÿ, R.; Kwak, Y. ATRP with Alkyl Pseudohalides Acting as Initiators and Chain Transfer Agents: When ATRP and RAFT Polymerization Become One. *Isr. J. Chem.* **2012**, *52* (3−4), 288−305.
(26) Nicolaÿ, R.; Kwak, Y.; Matyjaszewski, K. A Green Route to Well-Defined High-Molecular-Weight (Co)polymers Using ARGET ATRP with Alkyl Pseudohalides and Copper Catalysis. *Angew. Chem., Int. Ed.* **2010**, *49* (3), 541−544.
(27) Zhang, Y.; Schröder, K.; Kwak, Y.; Krys, P.; Morin, A. N.; Pintauer, T.; Poli, R.; Matyjaszewski, K. Reversible-Deactivation Radical Polymerization of Methyl Methacrylate and Styrene Mediated by Alkyl Dithiocarbamates and Copper Acetylacetonates. *Macromolecules* **2013**, *46* (14), 5512−5519.
(28) Wang, Y.; Fantin, M.; Matyjaszewski, K. Electrochemically mediated atom transfer radical polymerization with dithiocarbamates as alkyl pseudohalides. *J. Polym. Sci., Part A: Polym. Chem.* **2019**, *57* (3), 376−381.
(29) Elsen, A. M.; Nicolaÿ, R.; Matyjaszewski, K. Dual Concurrent ATRP/RAFT of Methyl Acrylate Co-initiated by Alkyl Halides. *Macromolecules* **2011**, *44* (7), 1752−1754.
(30) Wang, Y.; Fantin, M.; Matyjaszewski, K. Synergy between Electrochemical ATRP and RAFT for Polymerization at Low Copper Loading. *Macromol. Rapid Commun.* **2018**, *39* (12), 1800221.
(31) Lovell, P. A.; Schork, F. J. Fundamentals of Emulsion Polymerization. *Biomacromolecules* **2020**, *21* (11), 4396−4441.
(32) Wang, Y.; Lorandi, F.; Fantin, M.; Matyjaszewski, K. Atom transfer radical polymerization in dispersed media with low-ppm catalyst loading. *Polymer* **2023**, *275*, 125913.
(33) Min, K.; Matyjaszewski, K. Atom transfer radical polymerization in aqueous dispersed media. *Central European Journal of Chemistry* **2009**, *7* (4), 657−674.
(34) Cunningham, M. F. Controlled/living radical polymerization in aqueous dispersed systems. *Prog. Polym. Sci.* **2008**, *33* (4), 365−398.
(35) Cunningham, M. F. Living/controlled radical polymerizations in dispersed phase systems. *Prog. Polym. Sci.* **2002**, *27* (6), 1039−1067.
(36) Thickett, S. C.; Gilbert, R. G. Emulsion polymerization: State of the art in kinetics and mechanisms. *Polymer* **2007**, *48* (24), 6965−6991.
(37) Chern, C. S. Emulsion polymerization mechanisms and kinetics. *Prog. Polym. Sci.* **2006**, *31* (5), 443−486.
(38) Asua, J. M. Emulsion polymerization: From fundamental mechanisms to process developments. *J. Polym. Sci., Part A: Polym. Chem.* **2004**, *42* (5), 1025−1041.
(39) Gaynor, S. G.; Qiu, J.; Matyjaszewski, K. Controlled/"living" radical polymerization applied to water-borne systems. *Macromolecules* **1998**, *31* (17), 5951−5954.
(40) Luo, Y.; Cui, X. Reversible addition-fragmentation chain transfer polymerization of methyl methacrylate in emulsion. *J. Polym. Sci., Part A: Polym. Chem.* **2006**, *44* (9), 2837−2847.
(41) McCormick, C. L.; Lowe, A. B. Aqueous RAFT Polymerization: Recent Developments in Synthesis of Functional Water-Soluble (Co)polymers with Controlled Structures. *Acc. Chem. Res.* **2004**, *37* (5), 312−325.
(42) Rizzardo, E.; Chen, M.; Chong, B.; Moad, G.; Skidmore, M.; Thang, S. H. RAFT Polymerization: Adding to the Picture. *Macromol. Symp.* **2007**, *248* (1), 104−116.
(43) Hill, M. R.; Carmean, R. N.; Sumerlin, B. S. Expanding the Scope of RAFT Polymerization: Recent Advances and New Horizons. *Macromolecules* **2015**, *48* (16), 5459−5469.
(44) Moad, G. RAFT Polymerization - Then and Now. *ACS Symp. Ser.* **2015**, *1187*, 211−246.
(45) Wang, Y.; Dadashi-Silab, S.; Matyjaszewski, K. Photoinduced Miniemulsion Atom Transfer Radical Polymerization. *ACS Macro Lett.* **2018**, *7* (6), 720−725.
(46) Wang, Y.; Dadashi-Silab, S.; Lorandi, F.; Matyjaszewski, K. Photoinduced atom transfer radical polymerization in ab initio emulsion. *Polymer* **2019**, *165*, 163−167.
(47) Szczepaniak, G.; Lagodzinska, M.; Dadashi-Silab, S.; Gorczynski, A.; Matyjaszewski, K. Fully oxygen-tolerant atom transfer radical polymerization triggered by sodium pyruvate. *Chem. Sci.* **2020**, *11* (33), 8809−8816.
(48) Szczepaniak, G.; Łagodzińska, M.; Dadashi-Silab, S.; Gorczyński, A.; Matyjaszewski, K. Fully oxygen-tolerant atom transfer radical polymerization triggered by sodium pyruvate. *Chemical Science* **2020**, *11* (33), 8809−8816.
(49) Enciso, A. E.; Fu, L.; Russell, A. J.; Matyjaszewski, K. A Breathing Atom-Transfer Radical Polymerization: Fully Oxygen-Tolerant Polymerization Inspired by Aerobic Respiration of Cells. *Angew. Chem., Int. Ed. Engl.* **2018**, *57* (4), 933−936.
(50) De Bon, F.; Fonseca, R. G.; Lorandi, F.; Serra, A. C.; Isse, A. A.; Matyjaszewski, K.; Coelho, J. F. J. The scale-up of electrochemically mediated atom transfer radical polymerization without deoxygenation. *Chem. Eng. J.* **2022**, *445*, 136690.
(51) Lorandi, F.; Wang, Y.; Fantin, M.; Matyjaszewski, K. Ab Initio Emulsion Atom-Transfer Radical Polymerization. *Angew. Chem., Int. Ed. Engl.* **2018**, *57* (27), 8270−8274.
(52) Bang, J.; Kim, S. H.; Drockenmuller, E.; Misner, M. J.; Russell, T. P.; Hawker, C. J. Defect-free nanoporous thin films from ABC triblock copolymers. *J. Am. Chem. Soc.* **2006**, *128* (23), 7622−7629.
(53) Perrier, S.; Takolpuckdee, P.; Westwood, J.; Lewis, D. M. Versatile chain transfer agents for reversible addition fragmentation chain transfer (RAFT) polymerization to synthesize functional polymeric architectures. *Macromolecules* **2004**, *37* (8), 2709−2717.
(54) Keddie, D. J.; Moad, G.; Rizzardo, E.; Thang, S. H. RAFT Agent Design and Synthesis. *Macromolecules* **2012**, *45* (13), 5321−5342.
(55) Zhou, X.; Ni, P.; Yu, Z. Comparison of RAFT polymerization of methyl methacrylate in conventional emulsion and miniemulsion systems. *Polymer* **2007**, *48* (21), 6262−6271.
(56) Moad, G. Mechanism and Kinetics of Dithiobenzoate-Mediated RAFT Polymerization - Status of the Dilemma. *Macromol. Chem. Phys.* **2014**, *215* (1), 9−26.
(57) Chapman, R.; Jung, K.; Boyer, C. Photo RAFT Polymerization. *RAFT Polymerization* **2021**, 611−645.
(58) McKenzie, T. G.; Fu, Q.; Wong, E. H. H.; Dunstan, D. E.; Qiao, G. G. Visible Light Mediated Controlled Radical Polymerization in the Absence of Exogenous Radical Sources or Catalysts. *Macromolecules* **2015**, *48* (12), 3864−3872.
(59) Xu, J.; Shanmugam, S.; Corrigan, N. A.; Boyer, C. Catalyst-Free Visible Light-Induced RAFT Photopolymerization. *ACS Symp. Ser.* **2015**, *1187*, 247−267.
(60) Thomas, D. B.; Convertine, A. J.; Hester, R. D.; Lowe, A. B.; McCormick, C. L. Hydrolytic susceptibility of dithioester chain transfer

agents and implications in aqueous RAFT polymerizations. *Macromolecules* **2004**, *37* (5), 1735−1741.
(61) da M. Costa, L. P.; McKenzie, T. G.; Schwarz, K. N.; Fu, Q.; Qiao, G. G. Observed Photoenhancement of RAFT Polymerizations under Fume Hood Lighting. *ACS Macro Lett.* **2016**, *5* (11), 1287−1292.
(62) Fantin, M.; Isse, A. A.; Gennaro, A.; Matyjaszewski, K. Understanding the Fundamentals of Aqueous ATRP and Defining Conditions for Better Control. *Macromolecules* **2015**, *48* (19), 6862−6875.
(63) Flejszar, M.; Ślusarczyk, K.; Hochół, A.; Chmielarz, P.; Spilarewicz, K.; Błoniarz, P. Replacing organics with water: Macromolecular engineering of non-water miscible poly(meth)acrylates via interfacial and ion-pair catalysis SARA ATRP in miniemulsion. *Eur. Polym. J.* **2023**, *197*, 112374.
(64) Yin, R.; Chmielarz, P.; Zaborniak, I.; Zhao, Y.; Szczepaniak, G.; Wang, Z.; Liu, T.; Wang, Y.; Sun, M.; Wu, H.; Tarnsangpradit, J.; Bockstaller, M. R.; Matyjaszewski, K. Miniemulsion SI-ATRP by Interfacial and Ion-Pair Catalysis for the Synthesis of Nanoparticle Brushes. *Macromolecules* **2022**, *55* (15), 6332−6340.
(65) Zaborniak, I.; Chmielarz, P. Miniemulsion switchable electrolysis under constant current conditions. *Polym. Adv. Technol.* **2020**, *31* (11), 2806−2815.
(66) Surmacz, K.; Chmielarz, P. Low Ppm Atom Transfer Radical Polymerization in (Mini)Emulsion Systems. *Materials (Basel)* **2020**, *13* (7), 1717.
(67) De Bon, F.; B. Barbosa, A.; Fonseca, R. G.; Fantin, M.; Serra, A. C.; F. J Coelho, J. Large volume and oxygen tolerant photoinduced aqueous atom transfer radical polymerization. *Chem. Eng. J.* **2023**, *451*, 138777.
(68) Fantin, M.; Chmielarz, P.; Wang, Y.; Lorandi, F.; Isse, A. A.; Gennaro, A.; Matyjaszewski, K. Harnessing the interaction between surfactant and hydrophilic catalyst to control eATRP in miniemulsion. *Macromolecules* **2017**, *50* (9), 3726−2732.
(69) Fantin, M.; Park, S.; Wang, Y.; Matyjaszewski, K. Electrochemical Atom Transfer Radical Polymerization in Miniemulsion with a Dual Catalytic System. *Macromolecules* **2016**, *49* (23), 8838−8847.
(70) Halnan, L. F.; Napper, D. H.; Gilbert, R. G. A study of the kinetics of the emulsion polymerization of butyl methacrylate. *Journal of the Chemical Society, Faraday Transactions 1: Physical Chemistry in Condensed Phases* **1984**, *80* (10), 2851−2865.
(71) Fantin, M.; Isse, A. A.; Matyjaszewski, K.; Gennaro, A. ATRP in Water: Kinetic Analysis of Active and Super-Active Catalysts for Enhanced Polymerization Control. *Macromolecules* **2017**, *50* (7), 2696−2705.
(72) Lorandi, F.; Fantin, M.; Shanmugam, S.; Wang, Y.; Isse, A. A.; Gennaro, A.; Matyjaszewski, K. Toward Electrochemically Mediated Reversible Addition-Fragmentation Chain-Transfer (eRAFT) Polymerization: Can Propagating Radicals Be Efficiently Electrogenerated from RAFT Agents? *Macromolecules* **2019**, *52* (4), 1479−1488.
(73) Strover, L. T.; Postma, A.; Horne, M. D.; Moad, G. Anthraquinone-Mediated Reduction of a Trithiocarbonate Chain-Transfer Agent to Initiate Electrochemical Reversible Addition-Fragmentation Chain Transfer Polymerization. *Macromolecules* **2020**, *53* (23), 10315−10322.
(74) Ribelli, T. G.; Lorandi, F.; Fantin, M.; Matyjaszewski, K. Atom Transfer Radical Polymerization: Billion Times More Active Catalysts and New Initiation Systems. *Macromol. Rapid Commun.* **2019**, *40* (1), No. e1800616.
(75) Wang, Y.; Lorandi, F.; Fantin, M.; Chmielarz, P.; Isse, A. A.; Gennaro, A.; Matyjaszewski, K. Miniemulsion ARGET ATRP via Interfacial and Ion-Pair Catalysis: From ppm to ppb of Residual Copper. *Macromolecules* **2017**, *50* (21), 8417−8425.
(76) Tang, W.; Matyjaszewski, K. Effect of Ligand Structure on Activation Rate Constants in ATRP. *Macromolecules* **2006**, *39* (15), 4953−4959.
(77) Enciso, A. E.; Lorandi, F.; Mehmood, A.; Fantin, M.; Szczepaniak, G.; Janesko, B. G.; Matyjaszewski, K. p-Substituted Tris(2-pyridylmethyl)amines as Ligands for Highly Active ATRP Catalysts: Facile Synthesis and Characterization. *Angew. Chem., Int. Ed. Engl.* **2020**, *59* (35), 14910−14920.
(78) Nanda, A. K.; Matyjaszewski, K. Effect of Penultimate Unit on the Activation Process in ATRP. *Macromolecules* **2003**, *36* (22), 8222−8224.
(79) Iliopoulos, K.; Krupka, O.; Gindre, D.; Salle, M. Reversible two-photon optical data storage in coumarin-based copolymers. *J. Am. Chem. Soc.* **2010**, *132* (41), 14343−5.
(80) Garrison, J. B.; Hughes, R. W.; Sumerlin, B. S. Backbone Degradation of Polymethacrylates via Metal-Free Ambient-Temperature Photoinduced Single-Electron Transfer. *ACS Macro Lett.* **2022**, *11* (4), 441−446.
(81) Garrison, J. B.; Hughes, R. W.; Young, J. B.; Sumerlin, B. S. Photoinduced SET to access olefin-acrylate copolymers. *Polym. Chem.* **2022**, *13* (7), 982−988.
(82) Young, J. B.; Hughes, R. W.; Tamura, A. M.; Bailey, L. S.; Stewart, K. A.; Sumerlin, B. S. Bulk depolymerization of poly(methyl methacrylate) via chain-end initiation for catalyst-free reversion to monomer. *Chem.* **2023**, *9* (9), 2669−2682.
(83) Frech, S.; Molle, E.; Hub, C.; Theato, P. Decarboxylation of Poly[N-(acryloyloxy)phthalimide] as a Versatile Tool for Post-polymerization Modification. *Macromol. Rapid Commun.* **2022**, *43* (10), No. e2200068.
(84) Fairbanks, B. D.; Gunatillake, P. A.; Meagher, L. Biomedical applications of polymers derived by reversible addition - fragmentation chain-transfer (RAFT). *Adv. Drug Deliv Rev.* **2015**, *91*, 141−52.
(85) Jesson, C. P.; Pearce, C. M.; Simon, H.; Werner, A.; Cunningham, V. J.; Lovett, J. R.; Smallridge, M. J.; Warren, N. J.; Armes, S. P. H(2)O(2) Enables Convenient Removal of RAFT End-Groups from Block Copolymer Nano-Objects Prepared via Polymerization-Induced Self-Assembly in Water. *Macromolecules* **2017**, *50* (1), 182−191.
(86) Langerman, M.; Hetterscheid, D. G. H. Mechanistic Study of the Activation and the Electrocatalytic Reduction of Hydrogen Peroxide by Cu-tmpa in Neutral Aqueous Solution. *ChemElectroChem.* **2021**, *8* (15), 2783−2791.
(87) Langerman, M.; Hetterscheid, D. G. H. Fast Oxygen Reduction Catalyzed by a Copper(II) Tris(2-pyridylmethyl)amine Complex through a Stepwise Mechanism. *Angew. Chem., Int. Ed. Engl.* **2019**, *58* (37), 12974−12978.
(88) Dietrich, M.; Glassner, M.; Gruendling, T.; Schmid, C.; Falkenhagen, J.; Barner-Kowollik, C. Facile conversion of RAFT polymers into hydroxyl functional polymers: a detailed investigation of variable monomer and RAFT agent combinations. *Polym. Chem.* **2010**, *1* (5), 634.

https://doi.org/10.1021/acs.macromol.4c01812
Macromolecules 2024, 57, 10297−10310